Bioelectrochemistry 153 (2023) 108456

Contents lists available at ScienceDirect

Bioelectrochemistry

journal homepage: www.journals.elsevier.com/bioelectrochemistry

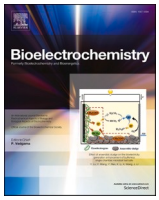

A non-faradaic impedimetric biosensor for monitoring of caspase 9 in mammalian cell culture

Boyang Chen *, Janice Kiely, Ibidapo Williams, Richard Luxton

Institute of Biosensing Technology, University of the West of England (UWE) Bristol, Frenchay Campus, Bristol BS16 1QY, UK

ARTICLE INFO

Keywords:
Apoptosis
Electrical impedance spectroscopy
Immunosensor
Caspase-9
Zinc oxide
Copper oxide

ABSTRACT

Lower yields and poorer quality of biopharmaceutical products result from cell death in bioreactors. Such cell death is commonly associated with programmed cell death or apoptosis. During apoptosis, caspases are activated and cause a cascade of events that eventually lead to cell destruction. We report on an impedance spectroscopy measurement technique for the detection of total caspase-9 in buffer and complex fluids, such as cell culture media. Enhanced sensitivity is achieved by leveraging the physiochemical properties of zinc oxide and copper oxide at the electrode-solution interface. Characterisation of the biosensor surface was performed using scanning electron microscopy and indirectly using an enzyme-linked immunosorbent assay. The characteristic biomolecular interactions between the target analyte and specific capture probe of the biosensor are quantified using non-faradaic electrical impedance spectroscopy (nfEIS). The proof-of-concept biosensor demonstrated a detection limit of 0.07 U/mL (0.032 μM) in buffer. The sensor requires a low sample volume of 50 μL without the need for sample dilution facilitating rapid analysis. Using a luminescence-based assay, the presence of active caspase-9 was detected in the culture media following exposure to a pro-apoptotic agent. We envision that the caspase-9 biosensor will be useful as a cell stress screening device for apoptosis monitoring.

1. Introduction

Mammalian cell cultures are the preferred expression hosts for the production of glycosylated recombinant proteins due to their ability to ensure proper protein folding and post-translational modification. Chinese hamster ovary (CHO) cells are arguably the most important, as it is estimated up to 70 % of all therapeutics employ CHO cell platforms, producing over $140 billion annually [1]. Researchers have explored optimisation strategies involving genetic modification of cell lines and alteration of culture media and bioreactor conditions, which usually seek to improve culture longevity, cell density, cell viability or protein productivity. However, many cell lines undergo apoptotic cell death in response to the stressful culture environment in bioreactors [2].

Nutrient limitation is one of the primary causes of cell death during the stationary phase and death phase. Other possible causes of cell death include hypoxia, toxic waste accumulation and mechanical agitation in the hydrodynamic environment [3]. Regardless of how apoptosis is triggered, it poses a major limiting factor in the production of recombinant proteins in cell cultures [4]. Ongoing cell death in the bioreactor hinders the ability to sustain a high-density culture with high viability. In addition, cell death results in release of cellular debris and proteases into the medium, which can complicate downstream purification processes and negatively affect the product quality [5]. Surprisingly, normal mammalian cells can escape late stage apoptosis if cell death stimulus is removed [6]. Partially deformed cells with obvious apoptotic morphologies can repair themselves after passing important checkpoints, including cytochrome *c* release, caspase activation, DNA damage, nuclear condensation and fragmentation [6]. Hence, the detection of apoptosis at its earliest stages will enable faster responses or pharmaceutical interventions to rescue the culture and enhance culture longevity and productivity.

Caspases belong to a family of cysteine proteases that play essential roles in apoptosis. Of the types of caspases, caspase-8, -9 and -3 have been suggested to be involved in the apoptotic cell death in batch and fed-batch cultures [7]. The intrinsic mitochondrial pathway is believed to be the dominant pathway in the initiation of apoptosis in non-induced CHO cell cultures, evidenced by data showing over 70 % of the culture expressing active caspase-9 compared to only 15 % expression of

* Corresponding author.
E-mail addresses: Boyang2.chen@live.uwe.ac.uk (B. Chen), Janice.Kiely@uwe.ac.uk (J. Kiely), Ibidapo.Williams@uwe.ac.uk (I. Williams), Richard.Luxton@uwe.ac.uk (R. Luxton).

https://doi.org/10.1016/j.bioelechem.2023.108456
Received 22 November 2022; Received in revised form 26 April 2023; Accepted 28 April 2023
Available online 2 May 2023

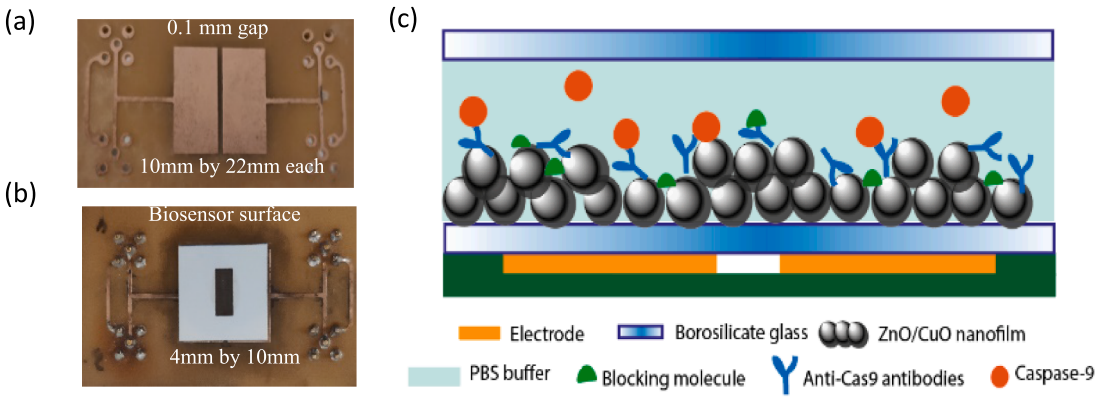

Fig. 1. Electrode setup and schematic of the biosensor (a) pair of square-shaped copper electrodes 22.1 mm diameter. (b) Sensor setup showing this sensing area (10 mm × 4 mm) defined by white tape. (c) Cross-sectional illustration of the biosensing surface and the biorecognition interactions between anti-cas9 and caspase-9.

caspase-8 and caspase-3 [4]. Caspase-9 is an important enzyme in the intrinsic apoptosis pathway, as caspase-9 can directly cleave and activate effector caspases-3 and caspase-7 [8]. Yun *et al.* [7] showed that specific inhibition of caspase-9 enhanced the viability of the CHO cells in both batch and fed-batch suspension cultures.

Techniques for the sensitive detection of caspases, such as fluorescence [9], colorimetry [10], chemiluminescence [11], photoelectrochemical [12], surface plasma resonance [13] and electrochemical methods [12,14–17], have been reported. Many of these methods exhibit high sensitivity, however, they involve multi-step and time-consuming processes, require expensive instruments and substrates and are also not suitable for rapid routine use. In contrast, electrochemical methods have been increasingly studied due to their low cost, rapid response, high sensitivity, simple operation and flexibility for miniaturisation [18,19]. Since caspases are proteases, they are able to recognise and cleave sequence-specific peptide substrates, which facilitates the development of protease assays [17,20]. Commonly, the sequence specific peptide is immobilised on an electrode surface through covalent interactions where caspase specific cleavage of the peptide leads to removal of the redox label [14]. This in turn results in a detectable change in Faradaic current or electrochemical impedance [14]. Unlike the faradaic methods, the non-faradaic method do not require redox probes, reference electrodes or a DC current [21]. In this technique, the biological interaction between the surface receptor and analyte gives rise to dielectric changes at the electrode surface, which can be assessed with impedance spectroscopy.

To improve detection sensitivity of electrochemical sensors, efforts have been made to amplify the signal with biological molecules and nanomaterials [14]. The use of nanomaterials with large surface area to volume ratios and high conductivity can increase the loading number of peptides or substrates on the electrode surface resulting in amplification of the electrical signal [14]. A typical n-type semiconductor such as zinc oxide (ZnO) when crystallised in its hexagonal (wurtzite) form, will exhibit special physiochemical properties, including high surface area, good biocompatibility, chemical stability and enhanced electron transport rate. For example, ZnO nanorods (<100 nm) boasts high surface-to-volume ratio allowing for a high loading density of proteins [22]. The high ionic strength and pH stability makes ZnO a suitable choice for biosensing in biological fluids where a reasonable lifetime is required [23,24]. In addition, most biological molecules are typically negatively charged and likely to interact with positively charged nanoparticles through electrostatic adsorption [23]. Recently, p-type materials such as copper oxide (CuO) have been shown to provide enhanced functionalities as counterparts of n-type materials through the formation of p-n junctions [25–28]. Lee *et al.* [25] presented a ZnO-CuO chemiresistive acetone sensor that comprises CuO nanocubes attached to ZnO nanospheres showing higher sensitivity than other acetone sensors. The interparticle p-n junctions resulted in increased resistance in response to reducing gases compared to p-p junctions alone. Composites of ZnO-CuO have also been used in protein sensing applications [26–28]. Batra *et al.* [28] deposited a ZnO-CuO composite matrix on to ITO coated glass substrate. The inclusion of the ZnO-CuO matrix facilitated faster electron transfer from the redox enzyme to the electrode surface [28].

Impedance spectroscopy is well suited for biological sensing since the binding of any biological entity (cells, proteins and DNA) results in unique impedance spectrum changes [28–31]. Previous studies have used standard faradaic methods to detect caspases, where the biorecognition molecules are immobilised directly onto the electrode surface [14,16,17]. *Xia et al.*[16] immobilised a biotinylated caspase-3 specific substrate on gold electrode surface. Once the substrate is cleaved by caspase-3, the biotin tag is detached from the surface leading to a decrease in electron transfer resistance, achieving a detection limit of 1 pg/mL [16]. The non-faradaic approach does not require the use of redox couple, this helps to avoid protein denaturisation caused by metallisation [32]. Additionally, the absence of redox probes enables more accurate and precise characterisation of biorecognition events at the electrode–electrolyte interface, where the interfacial capacitive changes should dominate [33,34]. This label-free and non-faradaic strategy has already been explored for the biosensing application of C-reactive protein (CRP) in buffer, and these biosensors were able to detection sub-ng/mL concentrations of CRP within ten minutes [26,27]. However, the application of this type of sensor for caspase detection and apoptosis monitoring in complex cell culture has not yet been investigated.

The present study investigates the feasibility of an impedimetric biosensor for the detection of caspase-9 in CHO cell culture. Intrinsic pathway is suggested to be a dominant trigger for apoptosis related cell death, as evidenced by a steep increase of activated caspase-9 early in the culture process [4,7]. The main focus for the fabrication of the biosensor was therefore the detection of caspase-9. The sensor surface consists of a mixture of ZnO and CuO nanocrystals for the immobilisation of anti-caspase-9 antibodies, shown in Fig. 1. Surface morphology were assessed using scanning electron microscopy (SEM) and cross-sectional images were taken to estimate the nanofilm height. Protein uptake on the nano-surfaces was detected and quantified using an enzyme-linked immunosorbent assay (ELISA). The ZnO/CuO nanocrystal surfaces were fabricated using an inexpensive colloidal dispersion technique and deposited on a glass substrate. The ZnO/CuO nanosurface was functionalised with anti-Cas 9 antibodies for the detection of caspase-9 in buffer. Staurosporine was used as a stressor for the initiation of apoptosis pathway in CHO-K1 cells and subsequent caspase production was assessed with impedimetric measurements. An equivalent electrical circuit model was developed to provide a detailed representation of the structure of our impedimetric sensor from a layer-by-

layer perspective. We envision the biosensor could be incorporated *in situ* to continuously measure apoptotic cell stress.

2. Materials and methods

2.1. Surface preparation

The sum of 0.3 g ZnO nanoparticles (99.9 +%, 80–200 nm from US Research Nanomaterials Inc. Houston, TX, USA) and 0.3 g of CuO nanoparticles (99.5 +%, width: 10–30 nm, length: 200–800 nm, US Research Nanomaterials Inc) was added to 30 mL double deionised water. The 1 % ZnO/1 % CuO suspension was stirred at room temperature for 1 h and then ultra-sonicated in pulsing mode (20 s off/20 s on) for 5 min using a 13 mm probe (Sonics & Materials. Inc.) at 100 W. Glass substrates were initially cleaned via sonication in ethanol for 10 min. 250 μL drops of the suspension were cast onto clean glass coverslips (width: 22 mm, length: 22 mm, thickness: 0.13–0.17 mm, Cole-Palmer, UK) to form ZnO/CuO nano-surfaces. Finally, they were dried in an oven at 50 °C for 4 h, then stored in a dry atmosphere with silica gel for up to 2 days.

2.2. Caspase 9 sensor fabrication

Rabbit anti-cleaved Caspase-9 IgG (ab52298, Abcam Ltd. UK) was stored and diluted in 0.01 M phosphate buffered saline (PBS, pH 7.3 ± 0.2 at 25 °C, Merck). The sensing area (10 mm × 4 mm) of each ZnO-CuO nano-surface on glass was defined by tape. Subsequently, 40 μL (1 μg/mL) of antibody solution was dropped on to the sensing area and incubated for 3 h at room temperature. Surfaces were washed three times with PBS buffer before the addition of 40 μL of 5 % non-fat milk to block the surface and inhibit nonspecific interactions. The surfaces were left at room temperature for 1 h and then washed again to remove unbound proteins. The biosensor was then dried in a vacuum desiccator with silica gel at 4 °C overnight for 18 h. The nano-surface biosensors were positioned above a pair of co-planar d-shaped electrodes formed from 35 μm copper on FR4 substrate (printed circuit board PCB). The overall diameter of the co-planar electrode is 22 mm, each electrode has a width of 10 mm and separation distance between the electrodes is 1.0 mm (Fig. 1a).The sensor was aligned in a way that the rectangular sensing area (10 mm × 4 mm) is positioned directly above the gap. A cross section of the biosensor is illustrated in Fig. 1c.

2.3. Surface characterisation

The ZnO/CuO nanocrystal surfaces were examined using a FEI Quanta FEG 650 field emission scanning electron microscope (ESEM) with a Low vacuum Secondary Electron (LFD) Detector operating in low vacuum mode. The surface morphology of ZnO coated nano-film and ZnO/CuO coated nano-film, were analysed. To perform the SEM analysis, samples were mounted on an aluminium stud and coated with a thin layer of Au using an Emscope SC500 Gold sputter unit prior to analysis. The cross-sections of the nanofilm were also examined using an Everhart-Thornley Detector (ETD), operating in high vacuum mode.

2.4. Surface uptake of antibody

Antibody uptake on ZnO-CuO nano-surfaces was quantified using an enzyme based immuno-assay. Using the ZnO-CuO nano-surfaces prepared as described previously, 50 μL (1 μg/mL) drops of mouse anti-cas9 IgG (sc-56073, Santa Cruz Biotechnology, Inc., USA) were cast onto the defined sensing area. The surfaces were then incubated for 3 h and then washed to remove unbound antibodies. The surfaces were incubated with 5 % non-fat milk for 1 h and washed again. The sensor was allowed to dry in a desiccator overnight. Following a thorough wash to remove any unbound antibody, 100 μL (1 μg/mL) of Goat anti-mouse IgG:HRP (Bio-Rad Laboratories Ltd, UK) was added to the surface and left for 1 h at 25 °C. Then, the surfaces were washed three times with PBS buffer to remove any unbound antibody. 200 μL of TMB (tetramethylbenzidine) (Alfa Aesar) solution was added as the enzyme substrate to generate a coloured product. Finally, 100 μL of the TMB solution were extracted from the sensor surface and mixed with 100 μL of TMB stop solution (Merck) inside 96 well plates. The intensity of the coloured product was read at 450 nm using a microplate reader (SpectraMax ID5, Molecular Devices).

2.5. Validation of antibody-protein interaction at the sensor surface

In order to validate the binding of caspase to our sensor surface, an assay based on sandwich ELISA was performed. The functionalised ZnO-CuO nano-surfaces were prepared as previously described in Section 2.2. Following a thorough wash step to remove unbound antibody and milk proteins, capase-9 spiked PBS solutions were added onto the surface and incubated for 30 min. Five concentrations of caspase-9 (0.1 U/mL, 0.25 U/mL, 0.5 U/mL, 1 U/mL and 2 U/mL) were studied. For control purposes, 50 μL of fresh PBS buffer without caspase-9 was added to the sensor surface. Following incubation with caspase-9 solutions, 50 μL (1 μg/mL) of mouse anti-cas9 IgG (sc-56073) was added to the sensor surface for 1 h to probe for any bound caspase-9. To probe for the mouse antibody, 100 μL (1 μg/mL) of goat anti-mouse IgG:HRP were added to the surface and left for 1 h. Finally, colour formation was generated from the TMB:HRP reaction was measured at 450 nm using a microplate reader.

2.6. Impedance measurements of caspase-9 in buffer

A HF2IS impedance Spectroscope with the HF2TA 50 MHz Current Amplifier (Zurich Instruments, Switzerland) was used to measure the impedance of the nano-crystal surfaces. The electrodes are insulated by the glass, no DC current can flow between the electrodes and therefore redox reactions are prevented. Four terminal impedance measurement mode was used to reduce the sensitivity of the measurement to connecting leads etc. In this mode, the HF2IS instrument generates a sine wave voltage excitation signal and the measured current and voltage drop across the sensor was used to calculate the impedance. The output voltage, Vz, was measured directly by the second differential of Input 1+ and input 1− of the HF2IS. The experimental setup is shown in Fig. S1. Impedance was measured from 15 MHz to 100 Hz at a voltage of 2 Vpp with 200 test points. An electrode voltage is applied to generate a sufficient electrostatic field beyond the glass layer in order to charge the zinc oxide substrate. The impedance plots were analysed using the ZiControl Frequency Response Analyzer tool.

The impedance amplitude and phase were measured after 5 min incubation time for 15 min following the addition of increasing concentrations (0, 0.1, 0.25, 0.5, 1 and 2 U/mL) of human recombinant active caspase-9 (CC120, Sigma-Aldrich). The sensing surface was washed with 0.01 M PBS and dried with paper towel before addition of each new sample. Damage to the sensor surface was minimised by carefully applying the paper towel to the edges of the sensing region and absorbing the liquid through capillary action. Sensor response was plotted using reading taken at a frequency of 6 MHz. Impedance amplitude, phase change and capacitance were evaluated as function of antigen (caspase-9) concentration in the buffer. The phase change was defined as the difference between the phase value of the biosensor after 10 min incubation with caspase-9 and the phase value of the control. Results were plotted using a logarithmic scale on the x axis.

To demonstrate specificity of the anti-cas9 antibody, control experiments consisting of 2 U/mL of caspase-3 (C1224, Sigma-Aldrich) and caspase-8 (C1099, Sigma-Aldrich) were added to the sensor surface functionalised with anti-cas9 antibody (ab2324).

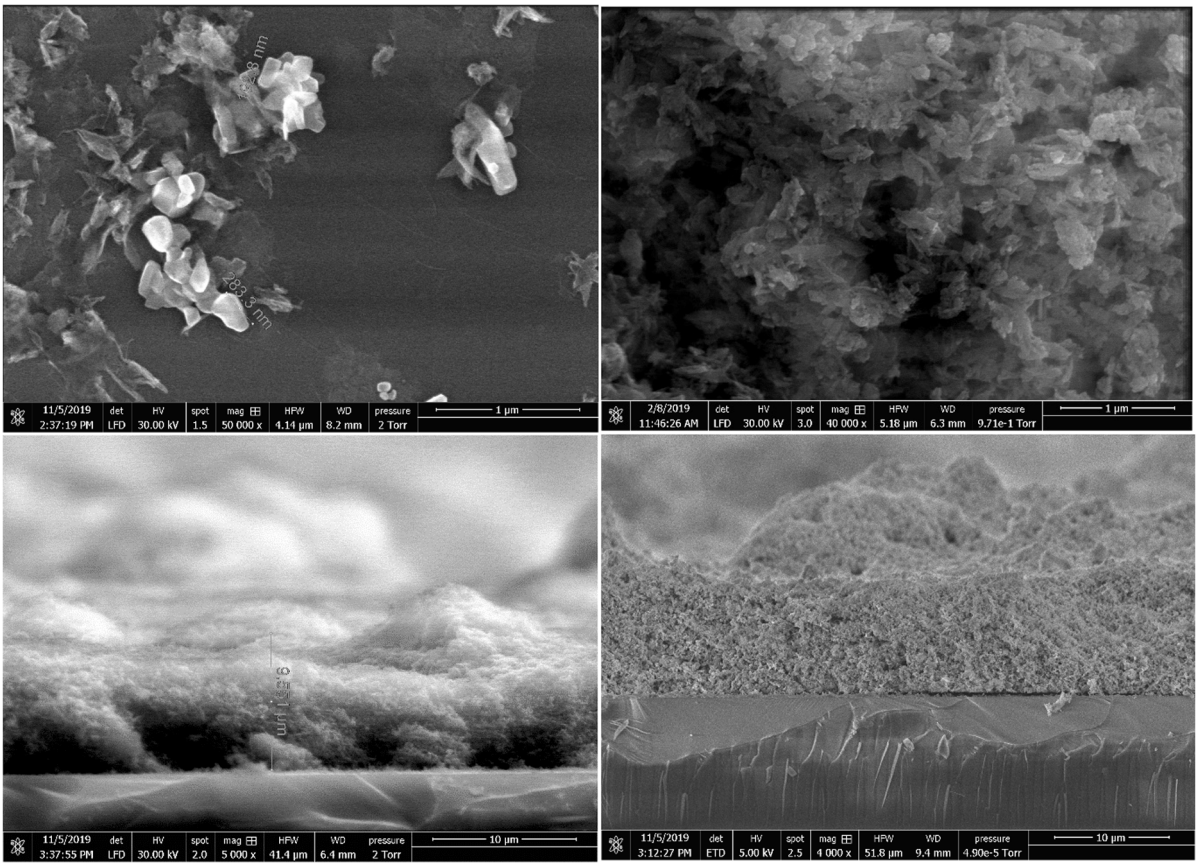

Fig. 2. Images captured using low vacuum secondary electron detector (LFD) for 1–1 ZnO-CuO nanocrystal surfaces. Approximate length of ZnO particles is displayed on the image. (a) 50,000× magnification. (b) 40,000× magnification. (c) Cross-sectional image of the nanocrystal sensor, nanofilm height is estimated. (d) Cross sectional image capture using ETD detector capturing the surface roughness of the nanocrystal film.

2.7. Induction of apoptosis

CHO-K1 cell lines (ATCC-CCL-61) were grown in F12K media (ATCC) supplemented with 10 % foetal bovine serum. They were maintained in T-75 flasks, incubated at 37 °C in a humified 5 % CO_2 atmosphere until 90 % confluency. CHO-K1 cells were counted and cell viability was calculated by Trypan blue dye exclusion using an automated cell counter (Luna II™; Logos Biosystems, Inc., Annandale, VA, USA). Cells were then seeded into 6 well plates and incubated at 37 °C for 24 h.

Staurosporine (19–123 M, Merck, UK) was diluted to produce a 1 mM stock solution. Following the 24 h incubation, cells were treated with 1 µM staurosporine and then incubated at 37 °C for 24 h. Cell images were captured using the Olympus SC50 industrial microscope camera fitted with a 20x objective lens (LCPLFLN20xLCD).

To extract the cell lysate, supernatant was removed from the cells, cells were then washed with PBS. The cells were then scraped from the flask. The sample was centrifuged at 1665 rpm for 5 min at 4 °C (Eppendorf Centrifuge 5804, A-4–44 swinging bucket rotor). The supernatant was then removed and discarded. The cell pellet was resuspended in 100 µL NP-40 Cell Lysis Buffer (Thermofisher) and incubated on ice for 10 min. Afterwards, samples were sonicated as follows: amplitude 50 %, 5 sec ON, 10 sec OFF, for a total sonication time of 1 min. Tubes were centrifuged at 8000 rpm for 15 min at 4 °C and supernatants were moved to quantification via EIS.

2.8. Bioimpedance measurements of caspase-9 in cell culture

ZnO-CuO biosensors were prepared as described in Section 2.2. Impedance amplitude, phase angle and capacitance measurements were taken on cell culture samples at 0, 1, 3, 4, 6 and 24 h following exposure to staurosporine. New sensors were used for the testing of subsequent samples. For control purposes, fresh F-12 K medium without cells were also studied. A Kruskal-Wallis test was used to analyse the data and level of significance was defined as $p \leq 0.05$.

2.9. Luminescence caspase activity assay

CHO-K1 cells were cultured in the same conditions as described in Section 2.7. In order to compare with the EIS data, chemiluminescent assays were carried out using a well-described Caspase-Glo® 9 Assay Systems from Promega (United Kingdom) following the manufacturer's recommended protocol. Briefly, the chemiluminescent assay was based on the luminescence of a p-nitroaniline (pNA) moiety that was released upon proteolytic activity of caspase-9 on a pNA-conjugate peptide substrate. The generated luminescence signal is correlated to the activity of caspase-9 present in the sample. Readings were taken at 0, 1, 3, 6 and 24 h following exposure to staurosporine. Six cell concentrations (5000, 10,000, 20,000, 40,000, 80,000 and 160,000 cells/50 µL) and five concentrations (1, 2, 4, 8 and 16 µM) of staurosporine were also studied. For control purposes, fresh F12-K medium with the peptide substrate only (without cells or toxins) were added to the control wells, and luminescence readings were measured using a microplate reader (SpectraMax ID5, Molecular Devices).

To determine the relationship between luminescence and caspase-9 activity. Caspase-9 activity was measured across different concentrations (0.1, 0.25, 0.5, 1, 2, 3, 4 U/mL) of caspase-9 (CC120). Caspase-9 was diluted in F12K media and incubated with an equal volume (50 µL) of Caspase-Glo® 9 reagent for 30 min at 37 °C. Luminescence readings were measured using a microplate reader.

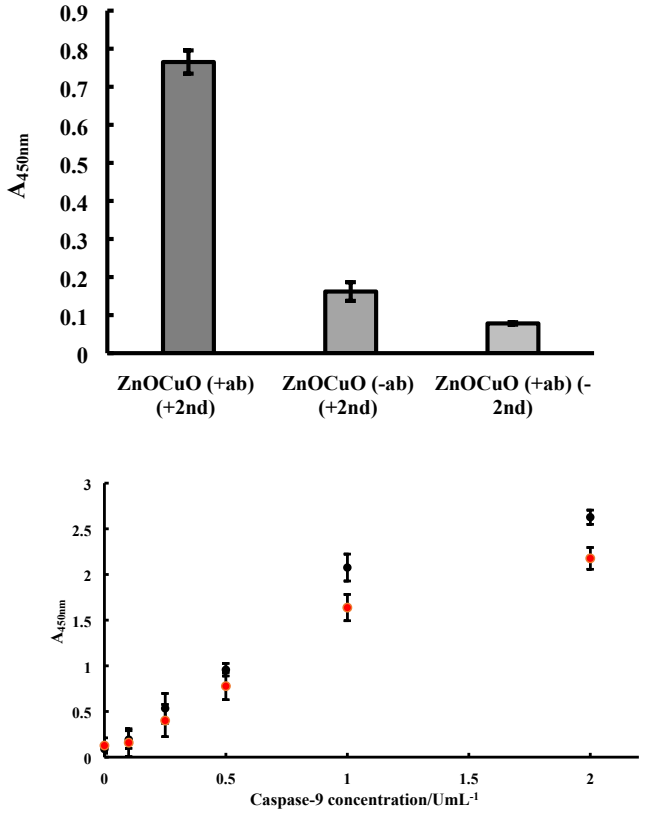

Fig. 3. Validation of nano-surface chemistry (a) Bar chart of anti-cas9 immobilisation on nano-surfaces expressed by colour formation at 450 nm from HRP-TMB reaction. Third bar: without secondary antibody. (b) Sandwich ELISA assay for the detection of caspase-9 binding. Antibody concentrations tested are 1 ug/mL (●) and 0.5 ug/mL (●). Standard error bars are shown (n = 5).

3. Results and discussions

3.1. Morphological and biochemical characterisation of sensor surface

3.1.1. Morphological characterisation of nano-surface using SEM

The ZnO/CuO composite nanoparticle surface deposited on the borosilicate substrate was characterised using SEM. Fig. 2a shows the columnar wurtzite structure of ZnO nanoparticles (width 80–200 nm). Fig. 2b illustrates that the CuO nanoparticles form smaller flake-like structures (width 30–40 nm) surrounding ZnO nanoparticles. A number of voids can be observed within this structure which can serve as additional sites for biomolecular interaction. The cross-sectional images of the nanocrystal film, shown in Fig. 2c and d, revealed an average film thickness of around 10 μm. The surface is rough as evidenced by the presence of peaks and valleys throughout the structure. The functionality of this type of biosensor is based around the conversion of binding events on the sensor surface into an electrical signal. Previously, greater surface roughness has been shown to be beneficial in biosensors. For example, Perry *et al.* [35] artificially introduced microcavities onto platinum electrode surface. This increases the electrode surface area, providing additional binding sites, which in turn provide faster rates of redox reactions relative to the smooth crystal faces [35].

3.1.2. Antibody functionalisation and validation

To validate the immobilisation of proteins on the ZnO-CuO nano-surfaces, an enzyme linked immunosorbent assay (ELISA) was performed (Section 2.4). Here, 1 μg/mL of anti-cas9 was added to the ZnO-CuO composite surfaces and a secondary antibody conjugated with horse radish peroxidase (HRP) was used to detect the specific protein binding on the nano-surfaces. The results shown in Fig. 3 indicate that the ZnO-CuO nano-surface was capable of capturing antibody even with the simple drying technique. The surfaces with antibody recorded an optical density (OD) of 0.76 compared to only 0.16 for surfaces without primary antibody. The high isoelectric points of ZnO (IEP ~ 9.5) [36] and CuO (IEP ~ 10) [37] enables stable immobilisation of biomolecules with lower IEP through electrostatic interaction. In contrast, IgG antibodies typically have a pI between 6.5 and 8.5 and are negatively charged at physiological pH [38]. Therefore, biomolecules can be readily immobilised on a positively charged ZnO through strong electrostatic interactions.

The sandwiched ELISA-based assay is used to validate the biomolecular binding of caspase-9 on the actual ZnO/CuO biosensor surface (Section 2.5). The measured absorbance values indicate caspase-9 binding can be detected on the sensor surface and the signal is linear between the concentration range of 0.1–1 U/mL (Fig. 3b). It can be seen that for the biosensors fabricated using 1 μg/mL generated larger output signals compared with the sensors fabricated with 0.5 μg/mL antibody, with greater differences at higher caspase-9 concentrations (Fig. 3b). This is to expected as there are more binding sites available for antigen capture resulting increased caspase-9 binding at the sensor surface and thus increased signal output. Two control experiment were conducted: one without the capture antibody produced an O.D of 0.238 and one without the secondary antibody produce an O.D of 0.088 (Fig. 3a). This indicates the change in colour intensity is due to the antibody-caspase-9 binding and not non-specific binding of the secondary antibody.

3.2. Detection of caspase 9 through bioimpedance measurements

3.2.1. Bioimpedance changes occur predominantly in mid-high frequency bands

Following the characterisation of the functionalised sensor surface with SEM and colorimetric assays, the specific binding interactions of caspase-9 were measured with electrical impedance spectroscopy. Impedance spectroscopy is a well-established approach for the analysis of complex biological liquids [39,40]. The sensor detects a variation of complex impedance, induced by dielectric constant change, the sensor response is mostly gained from a capacitive component of the complex impedance [40]. Previous publications have demonstrated that a capacitive mode can be preferable for measurement of an antibody capture of an antigen [41]. In a typical non-faradaic impedance plot, the absence of redox reaction eliminates the parameters in the Randles model associated with electron transfer i.e. charge transfer resistance (R_{ct}) and Warburg impedance (Z_w), as these tend to infinity. Therefore, in a non-faradaic EIS system, the impedance is inversely proportional to the electrical double layer capacitance.

For the characterisation of the biosensor performance, successive cycles of the immersion of the fixed protein solution and the corresponding impedance magnitude (|Z|), phase and capacitance measurements were performed for each caspase-9 concentration (0.1, 0.25, 0.5, 1 and 2 U/mL). The analysis of protein solutions was made over the frequency range of 100 Hz to 15 MHz encompassing both α (1 Hz–100 kHz) and β (100 kHz–10 MHz) dielectric dispersion regions [40] expected for the caspase-9 solution (n = 5). The experimental setup is shown in Fig. S1. In our R^2 correlation coefficient plot (Fig. S2), areas of high correlation could be observed at low (<1000 Hz) and high (>1 MHz) frequencies, although the correlations tended to be more sporadic at lower frequencies (Fig. S3). The coax connection and surrounding parasitic environment effects contribute significantly to the modulus of impedance at the lower frequencies. As shown in Fig. 4a and Fig. 4b, the mid-high frequency regions (100 kHz–10 MHz) appear to contain the most significant changes in both impedance magnitude and phase shift. This finding concurred with previous literature. For example, Oseev et al. [40] demonstrated the distinguishing sensor response on various protein concentrations in the frequency ranges of β (100 kHz–10 MHz) and δ (10 MHz–1 GHz) dispersion regions. A frequency of 6 MHz was selected for the calibration plots, because at this frequency, we

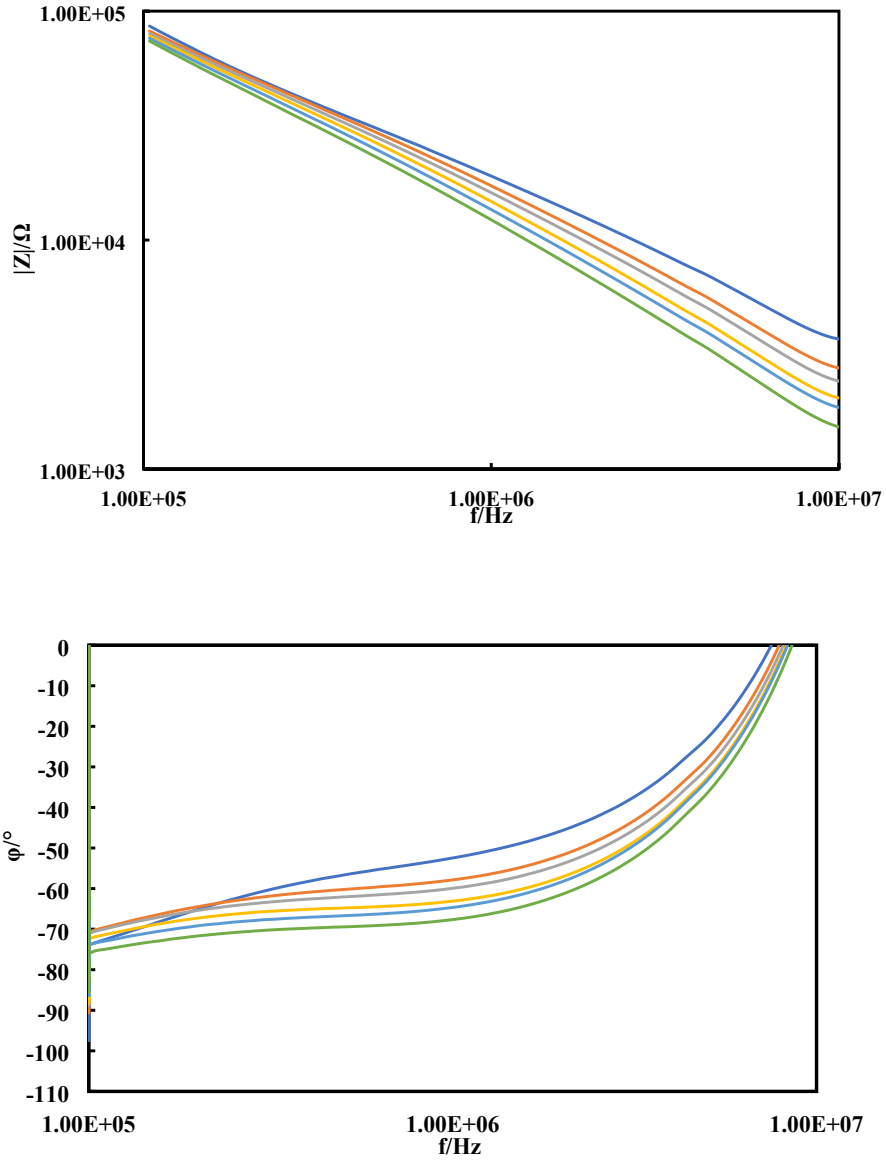

Fig. 4. Frequency dependent phase and impedance responses (a) Impedance magnitude spectra (100 kHz–10 MHz) of the biosensor coated with 1 % ZnO/CuO functionalised with 1 μg/mL anti-cas-9. Responses to caspase-9 loading at various concentrations: 0 (—), 0.1 (—), 0.25 (—), 0.5 (—), 1 (—) and 2 (—) U/mL, were recorded. (b) Equivalent phase plot (100 Hz–10 MHz).

calculated a significant statistical difference (2σ) between the buffer measurement (0 U/mL) and the first sample (0.1 U/mL).

3.2.2. Increased caspase-9 loading lead to decreases in impedance magnitude and phase angle

Fig. 5a shows the generated calibration curves containing the corresponding impedance and phase values with different concentrations (0, 0.1, 0.25, 0.5, 1, 2 U/mL) caspase-9 after 10 min incubation on the sensor surface measured at a frequency of 6 MHz (the mean of 5 replicates). Both impedance magnitude and phase angle decrease with caspase-9 concentration. There are several explanations of this phenomenon. Semiconductor materials, such as ZnO and CuO, will readily form an electrical double layer when they interact with the liquid electrolyte, resulting in charge accumulation at the interface region [26]. Furthermore, the binding interaction between the capture antibody and target biomolecule at the electrode surface results in a capacitive increase [39]. When caspase-9 antigen binds to the ZnO/CuO surface through capture by receptor antibody, a decrease in impedance is measured. These results indicate that there is increased negative charge accumulation due the effect of bound antigen's net charge. Therefore, the decrease in impedance can be interpreted as a decrease in overall positive charge with increased caspase-9 loading. This dominant capacitive behaviour can be observed in the Bode magnitude and phase plots in the ranges from 6000 Ω to 10,000 Ω from −50° to −70° in Fig. 4a and 4b respectively.

Using the logarithmic regression model on the capacitance data (Fig. 5b), the limit of detection (LOD) of the experiment was defined as 0.07 U/mL (0.032 μM) with a confidence level higher than 95 % when ± 2σ (0.286 pF) was considered. The regression line associated with the data from the sensor has a R^2 value of 0.9852, indicating high degree of correlation in the observed data. A statistical analysis of the impedance values taken at a frequency of 138 Hz is shown in Table S1. The inter-assay %CV is calculated to be 8.17 % demonstrating high degree of reproducibility.

It has been reported that an increase in protein load can result in a reduction in protein solution impedance [40]. To determine if this was the case, impedance measurements of caspase-9 were performed on non-functionalised surfaces. It can be seen from the dose response curves that

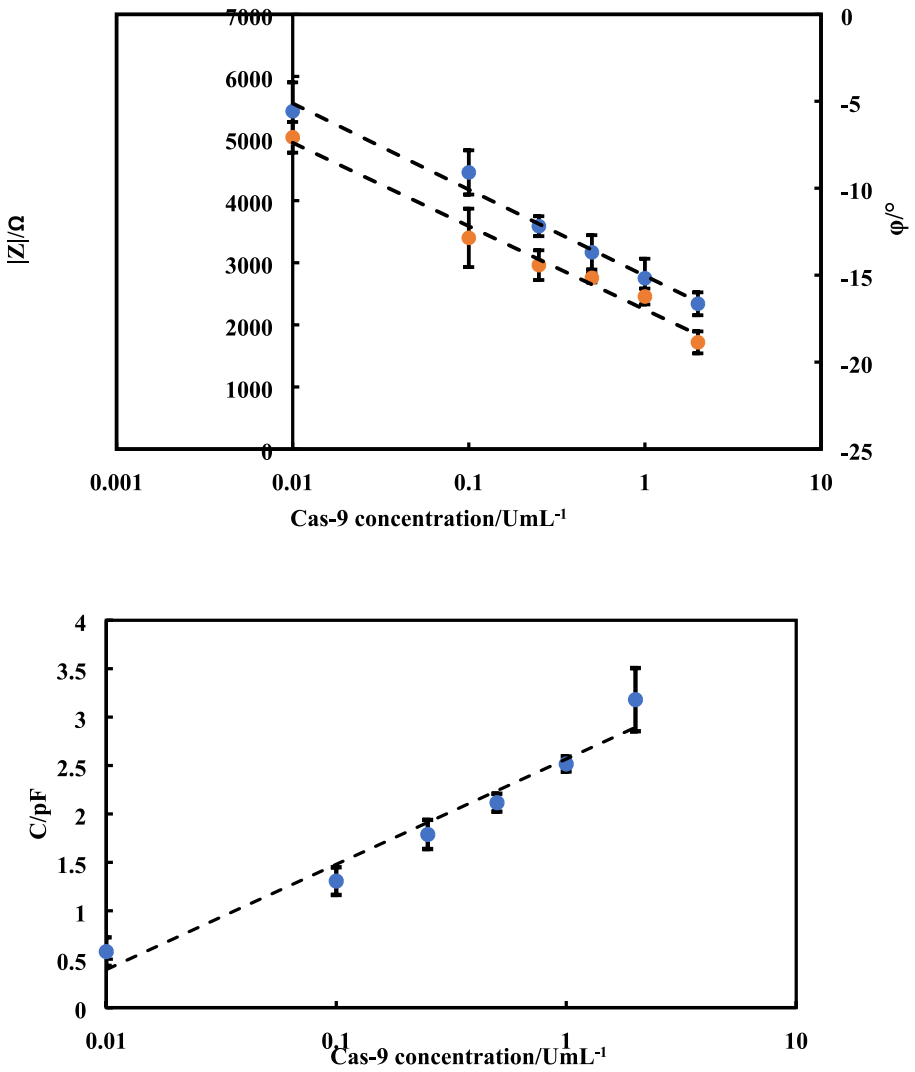

Fig. 5. (a) Impedance magnitude (•) and phase angle (•) values recorded at 6 MHz from sensor with 200 ng capture antibody tested with PBS spiked with increasing concentrations of caspase-9: 0, 0.1, 0.25, 0.5, 1, 2 U/mL. (b) Capacitance measurements vs caspase-9 concentration (0, 0.1, 0.25, 0.5, 1, 2 U/mL). (c) Impedance plot comparing the responses from cas-9 antibody (•), cleaved cas-9 antibody (•) and control (•). Control experiments were conducted without anti-cas-9 functionalisation. Because of logarithmic scale buffer reading is represented at 0.01 U/mL Cas-9 concentration. Error bars represent 1 standard deviation (n = 5). (d) Specificity of the caspase-9 (•) sensor. Interferents of caspase-3 (•) and caspase-8 (•) were tested. Error bars represent 1 standard deviation (n = 5).

there was a small reduction in impedance magnitude with the initial concentrations of caspase 9 (Fig. 5c). This was likely a result of non-specific interactions at the electrode–electrolyte interface caused by electrostatic interactions and other physical adsorption processes. However, despite this, the addition of recognition layer resulted in significantly larger signal outputs relative to the control, $p = 0.02$ (Kruskal-Wallis test).

The selectivity of the antibody-functionalized immunosensor for caspase-9 was tested *by* comparing the EIS signal changes brought about by two other caspase proteins: caspase-3 and caspase-8. Fig. 5d compares the EIS responses of the immunosensor for 0.5 and 2 U/mL of caspase-3 and caspase-8 solutions in the absence of caspase-9. The results showed that caspase-3 and caspase-8 did not exhibit any significant decrease in impedance magnitude. In contrast to the incubation of the immunosensor in 2 U/mL caspase-9, the resulting impedance greatly decreased. For both concentrations tested for caspase-3 and caspase-8, the resulting readings were not statistically significant compared to the buffer control ($p \leq 0.05$) (Fig. 5d).

3.2.3. *Equivalent electrical circuit modelling*

The explanation of obtained experimental results can be completed with the help of the appropriate equivalent circuits that simultaneously fit to the sensor design and to experimental dependencies (Fig. 6a). The equivalent circuit was deduced from the obtained experimental data presented in Fig. 5. The equivalent circuit model is shown in Fig. 6b. The data for each element of the equivalent circuit are summarised in Table 1.

The measured impedance change, identified as non-faradaic, is dominated by the capacitance of the double layer formed at the sensing electrode-fluid interface. And for the biosensor described in this work, the impedance change can be attributed to the change in number of binding events at the biosurface-solution interface. Small changes in the number of binding events can result in changes in capacitance (fF ~ pF changes). Similar capacitive biosensors have been reported [42], where two measurement electrodes are positioned underneath an insulating layer to measure the capacitance of the biosensor, as the dielectric properties of the solution changes with the total number of bio-recognition events.

The total capacitance of the sensor could be depicted as a network of

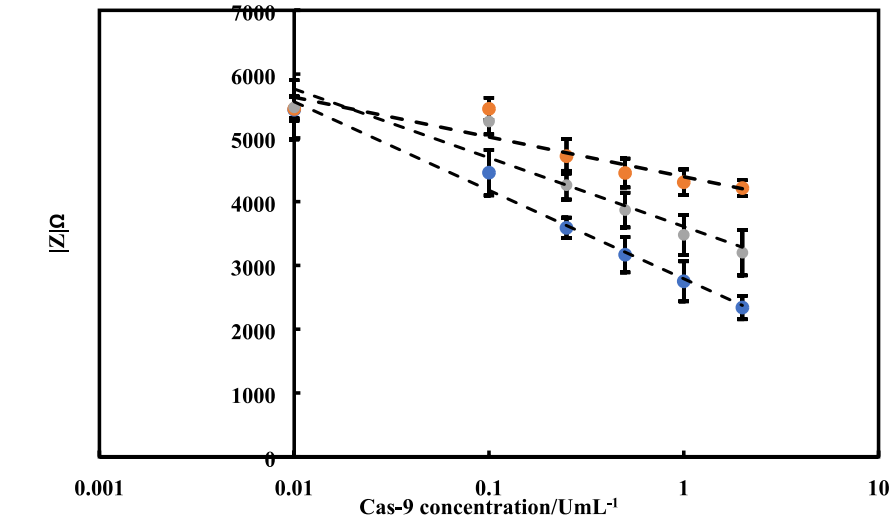

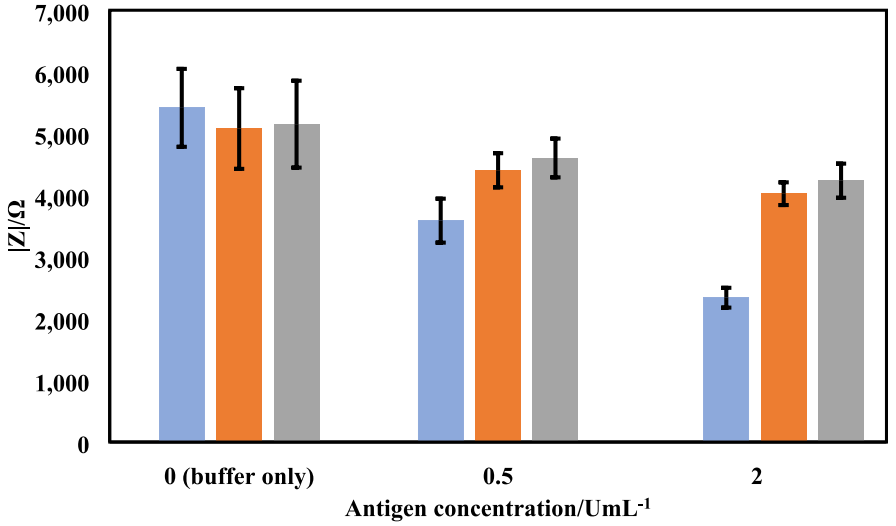

Fig. 5. (*continued*).

several capacitors. The first capacitor, C_{ins}, constitutes the insulating layer of borosilicate glass on the electrode surface and represents the fixed dielectric constant of the insulator capacitance. The second capacitor, C_{ZnO+AB}, includes the capacitance of the ZnO-CuO nanofilm and anti-caspase9 molecular layer and this represents the capacitance formed at the contact surface between the sensor and the bioreceptor layer. The third capacitor, C_{cas9}, represents a capacitance associated by the concentration-dependent biomolecular interactions between caspase-9 and its antibody at the biosensor surface. The bulk PBS impedance is modelled as parallel circuit containing C_{pbs} and R_{pbs}, capacitance and resistance (400 Ω, calculated from conductivity of the ionic solution). As can be seen in Table 1, the parameters prescribed to the caspase-9 binding events have the largest influence. At the highest concentration of caspase-9, the deduced capacitance values were 13-fold higher compared to the PBS only controls.

3.3. Detection of caspase-9 in the culture media

To test the impedimetric biosensor ability to detect caspase release in mammalian cell culture, CHO-K1 cells were subjected to a cell death stimulus (staurosporine) which can effectively trigger apoptosis [43]. Zhang et al. [44] demonstrated that CHO-K1 cells treated with staurosporine exhibit distinct apoptotic phenotypes including nuclear condensation, DNA fragmentation and cell shrinkage. These apoptotic phenotypes are associated with an increase in cellular caspase activity [44]. Staurosporine (1 μM final concentration) was added to the cell culture medium to initiate apoptosis.

Morphologic criteria are considered reliable evidence of apoptosis. However, demonstration of complete apoptotic morphology by a single method is difficult. Nuclear condensation, shrinkage of the cell and fragmentation into apoptotic bodies can be visualised using light microscopy [45]. Fig. 7 shows the clear difference in cell morphology between healthy CHO cells and staurosporine-treated cells. Within 6 h, condensation of cytoplasm, organelles and membrane and nuclear fragmentation (pyknosis) can be observed. Another key feature of apoptotic morphology is the separation of neighbouring cells and this is a result of cell shrinkage and cell death via secondary necrosis (Fig. 7c and 7d). Also to note, the asynchronous nature of apoptotic cell death in cell populations is mainly due to the variable duration of the initiation phase. As a result, imaging methods alone may not capture the true

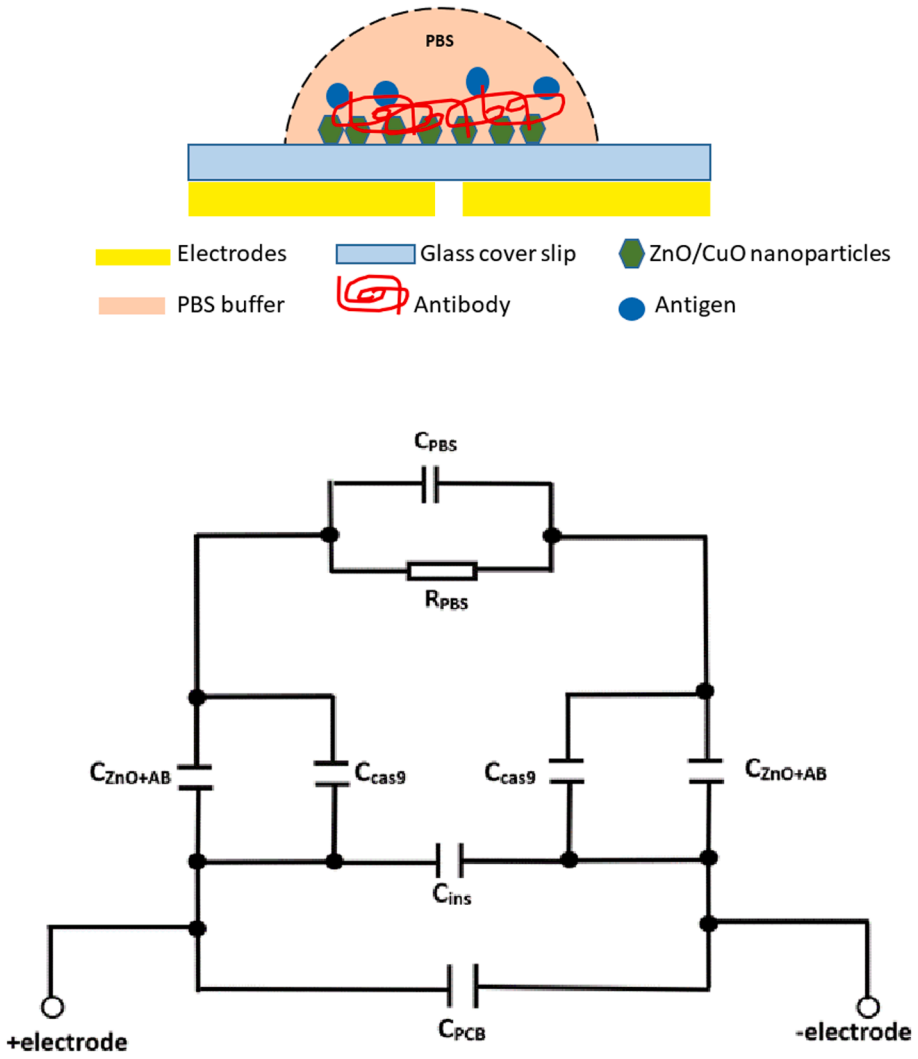

Fig. 6. (a) Schematic of the biosensor. (b) Equivalent circuit model for the biosensor. Measured capacitance comprised of three capacitors including the fixed capacitance of the insulator, C_{ins}, the interfacial capacitance associated with ZnO/CuO and caspase-9 antibodies, $C_{ZnO+ABl}$, the caspase-9 binding capacitance which reflects when the target protein binds to the capture antibody bound to the ZnO/CuO surface, C_{cas9}, and the PBS buffer bulk capacitance and resistance, C_{PBS} and R_{PBS}.

Table 1
Calculated capacitance values (at 6 MHz).

Equivalent component	PBS	PBS/ Cas9 [0.1 U/ mL]	PBS/ Cas9 [0.25 U/ mL]	PBS/ Cas9 [0.5 U/ mL]	PBS/ Cas9 [1 U/ mL]	PBS/ Cas9 [2 U/ mL]
C_{ins} [fF]	85.34	85.34	85.34	85.34	85.34	85.34
C_{ZnO+AB} [fF]	26.11	26.11	26.11	26.11	26.11	26.11
C_{cas9} [fF]	190.4	765.38	1246.88	1575.1	1974.65	2639.18

Footnote. Equivalent circuit components. C_{ins}: insulator capacitance, C_{ZnO+AB}: interfacial capacitance associated with ZnO/CuO and caspase-9 antibodies, C_{cas9}: caspase-9 binding capacitance.

extent of apoptotic progression across the entire cell population. Cell viability was assessed by trypan blue staining. The results show a significant drop (10 %) in viability after 3 h of staurosporine treatment (Fig. 7e). The untreated controls did not display any morphology signs of apoptosis or loss of cell viability.

For biochemical measurements for apoptosis, luminescent caspase-9 assays were performed using a commercially available test kit as described in the Experimental Section 2.9. The assay uses a luminogenic substrate containing a caspase specific sequence. Following caspase cleavage, amino-luciferin is released, resulting in the luciferase reaction and the production of light. The effect of staurosporine exposure on caspase-9 activity was monitored over a 24-hour timeframe (1, 3, 6 and 24 h). The signal generated is proportional to the amount of caspase activity present. A twofold increase in caspase-9 activity was observed following 6 h exposure to staurosporine (Fig. 8a). No significant change in caspase activity was detected in the control samples (Fig. 8a). The results are consistent with previous literature as Mokhtar *et al.* [46] measured a significant increase in LEHD-cleaving activity in HEK293T cells 4 h following apoptosis induction.

In a bioreactor, the extent of apoptotic stress will vary depending on the culture conditions. Here, we exposed the cells to various concentrations of staurosporine (1, 2, 4, 8, 16 μM) and assessed the resulting caspase activity. An increase in caspase activity was measured up to 4 μM staurosporine, however a decrease in luminescence signal was measured at high concentrations (Fig. 8b). This can be attributed to excessive stress exerted on to the CHO-K1 cells at high concentrations of staurosporine which leads to accelerated apoptosis and cell death. As cells enter late stages of apoptosis, early markers such as caspase-8 and −9 would no longer to be predominant in the culture.

To gain further insight into the staurosporine induced caspase activation and caspase release, we conducted an experiment using different starting cell numbers (5000, 10,000, 20,000, 40,000, 80,000, 160,000

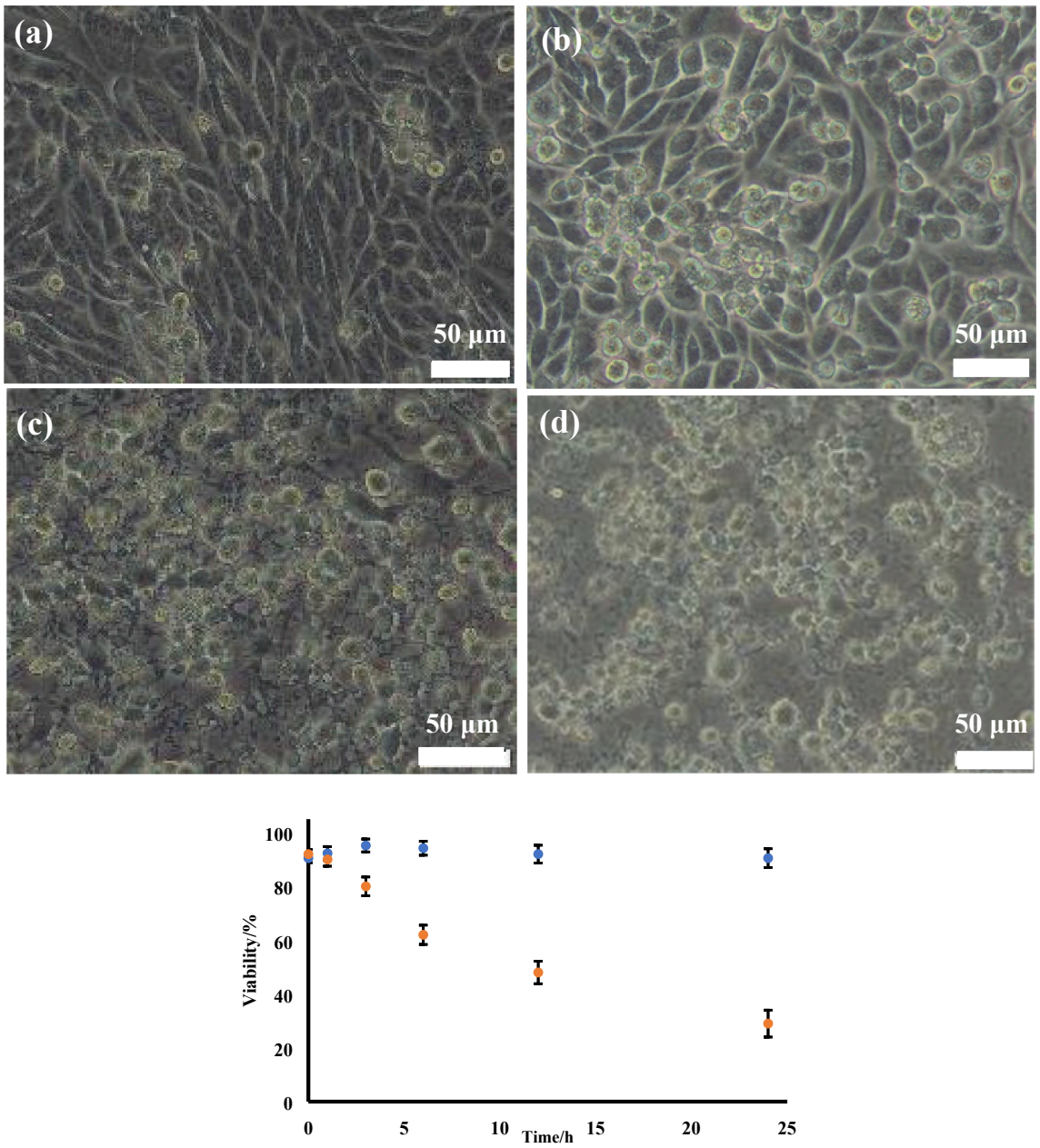

Fig. 7. Bright-field microscope images of CHO-K1 cells incubated for, (a) 6 h and (b) 24 h, at 37 °C. Images of CHO-K1 cells treated with 1 µM staurosporine and incubated for (c) 6 h and (d) 24 h, at 37 °C. (e) Cell viability assay analysis of staurosporine (1 µM) treated (•) and non-treated (•) CHO-K1 cells. Error bars (1 σ) are shown (n = 6).

cells/50 µL). These specific cell numbers were used to represent a high-density CHO culture process at the end of the exponential growth phase, as the culture becomes confluent and cell concentration reaches above 1,000,000 cells/mL. By varying the starting cell number, total caspase activity and production should differ in response to the same drug treatment. The results show a linear relationship between caspase activity and increasing cell number (Fig. 8c), this is reflective of increasing caspase concentration in the culture media and the staurosporine's toxic effect. In the untreated controls, caspase activity also increased with cell number but with significantly lower luminescence values (Fig. 8c). This is the baseline caspase activity as cells are undergoing the natural apoptotic process.

To determine the relationship between luminescence and caspase-9 activity, we measured the RFU values for each of the standard caspase-9 concentrations (0.1, 0.25, 0.5, 1, 2, 3, 4 U/mL). It can be seen from the plot, the luminescence values are linearly correlated with the concentration of caspase-9 in the range of 0.1–2 U/mL (Fig. 8d) and begin to level off when the concentrations reached 3 U/mL. A statistical analysis of the measured luminescence values for each concentration of caspase-9 is shown in Table S2. The average CV % is calculated to be 14.2 %. This result can be compared to the impedance data in Fig. 5, where the same concentration range was used, further highlighting the relationship between caspase activity and concentration.

3.4. Evaluation of caspase-9 in CHO culture with impedance spectroscopy

In order to demonstrate the applicability of the technique for early detection of apoptosis in live cell culture samples, we performed a timed study with the impedimetric biosensor to detect caspase-9 over a six-hour time frame. Following the initial addition of staurosporine, impedance magnitude measurements were taken at 6 MHz at regular intervals. The impedance signal response for each of the six time points

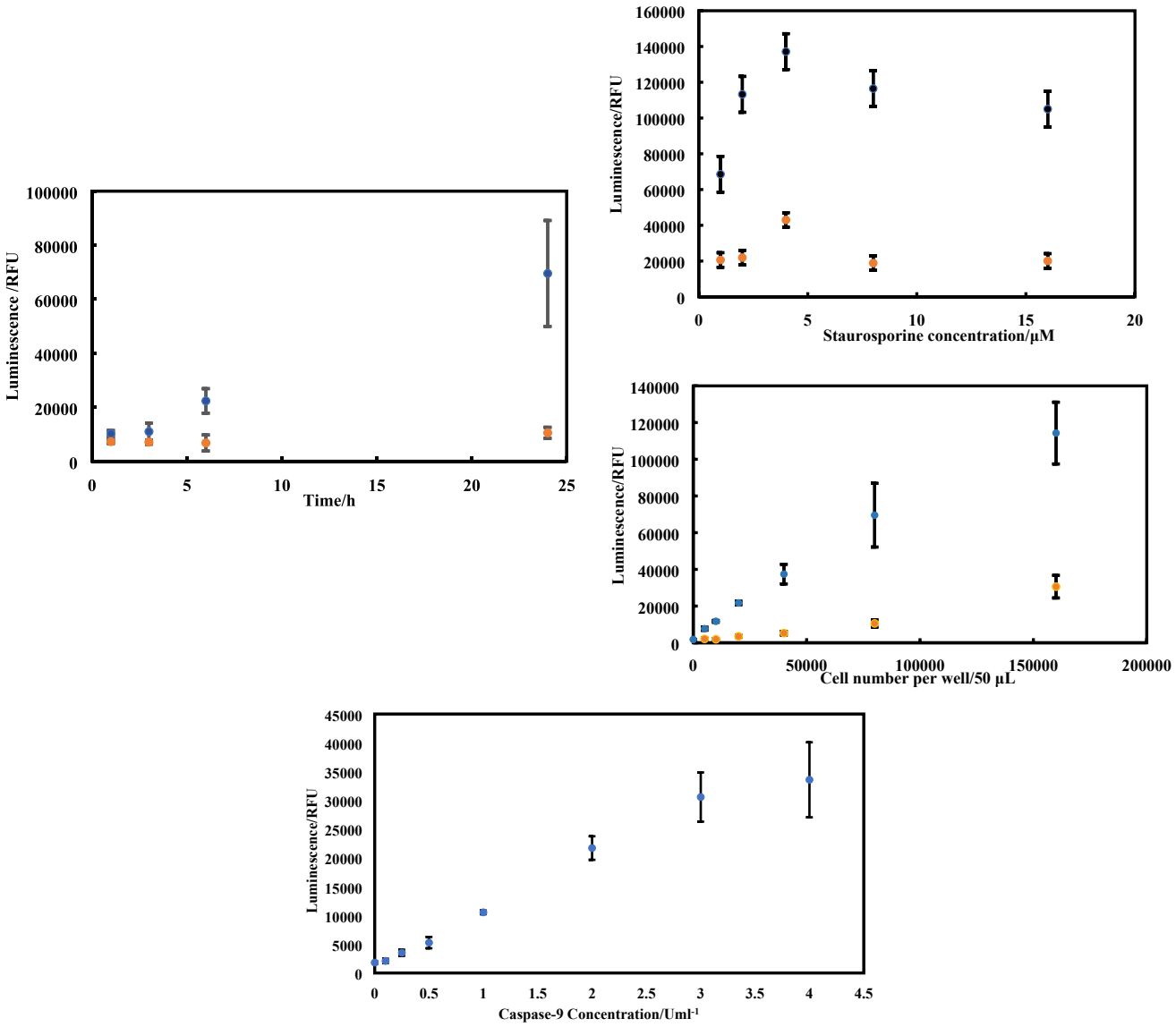

Fig. 8. Caspase activity assays. (a) CHO-K1 cells were subjected to 1 μM of staurosporine exposure for 1, 3, 6 and 24 h. (b) CHO-K1 cells were exposed to varying concentrations of staurosporine (1, 2, 4, 8 and 16 μM) for 24 h. (c) CHO-K1 (varying starting cell number) were subjected to 1 μM of staurosporine and incubated for 24 h. Treated (•) and untreated controls (•) were plotted and errors bars (1 σ) are shown (n = 5). Controls refer to the cell samples without exposure to staurosporine. (d) Caspase activity assay with standard concentrations of caspase-9 (0.1, 0.25, 0.5, 1, 2, 3, 4 U/mL). Error bars (1 σ) are shown (n = 6).

is shown in Fig. 9a. The decrease in impedance magnitude was evident following three hours of exposure to staurosporine, where the mean impedance values were significantly different from the untreated controls with a confidence level higher than 95 % (±2σ). This finding was consistent with the caspase activity assay results shown in Fig. 9b, as we found the levels of caspase-9 activity to increase linearly between 2 and 6 h. Background apoptotic activity is expected in the cell culture and cellular debris resulting from low level cell break-down detected which was detected through interactions on the sensor surface. This was shown to result in 9.8 % change in impedance over 6 h in our untreated culture samples (Fig. 9a). On the other hand, a 46.4 % change in impedance was recorded in the staurosporine samples over the same time frame (Fig. 9a).

Bio-impedance sensing and caspase activity assays were also performed for cell culture samples with defined cell concentrations and the relationship between caspase-9 activity and concentration was explored (Fig. 10). In this study, these specific cell numbers were used to represent a high-density CHO culture process at the end of the exponential growth phase, as the culture becomes confluent and cell concentration reaches above 1,000,000 cells/mL. From the caspase activity assay data, we demonstrated that an increase in the number of cells leads to an increase in caspase-9 activity (RFU readings) for a given toxic challenge (Fig. 10). The impedance behaviour was consistent with the results from the calibration curve data in Fig. 5, i.e. a decrease in impedance magnitude was measured with increasing caspase-9 concentration. The decrease in impedance reflects an increase in the overall capacitance of the system. This capacitance change is largely dominated by the charge accumulation as a result of antigen binding with antibody and to a lesser extent, an increase in polarity of the solution due to increased caspase-9 load [40,41].

We have successfully demonstrated the application of electrical impedance spectroscopy for the detection of early apoptotic markers in cell culture samples before clearly detectable morphological hallmarks are present.

4. Conclusions

We have successfully shown the application of bioimpedance

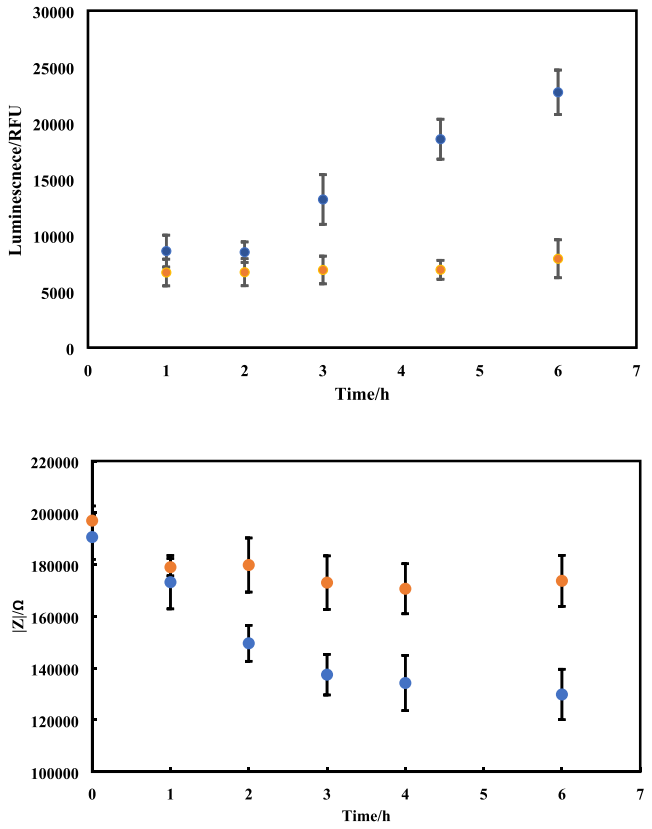

Fig. 9. Timed measurements of caspase-9 levels with impedance and caspase activity assay in the first six hours (a) Impedance analysis (6 MHz) of CHO-K1 cell culture samples following addition of 1 μM staurosporine. (b) Caspase activity recorded in CHO-K1 cell culture samples following addition of 1 μM staurosporine. Treated (•) and untreated controls (•) were plotted and errors bars (1 σ) are shown (n = 5).

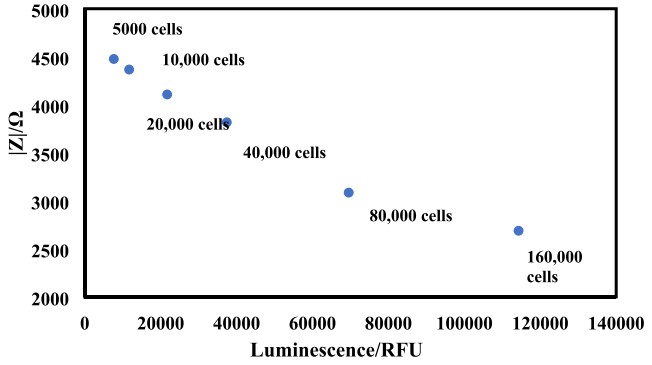

Fig. 10. Comparison between luminescence readings and impedance output (6 MHz) of CHO-K1 cell culture sample following 24-hour exposure to 1 μM staurosporine. Different starting cell numbers were tested. Higher luminescence reading (higher caspase-9 activity) is correlated with lower impedance output.

technology in the detection of apoptosis and experimentally confirmed the sensor's ability to measure caspase-9. The sensor is fabricated using a simple and inexpensive colloidal sonication technique. It is stable against electrode polarisation and capacitive artefacts especially for the analysis in the mid-high frequency ranges. The sensor was evaluated experimentally with different concentrations of caspase-9 protein solutions and with samples extracted from CHO cell culture. The performance of the biosensor was evaluated with impedance spectroscopy, with a limit of detection of around 0.07 U/mL being achieved and it was tested as a proof of concept with culture media spiked with increasing caspase-9 concentrations. The average analysis time (45 min including preparation) is shorter than commercial ELISA (at least 2.5 hrs). The sensor can be activated at a single frequency which would further lower the cost of instrumentation and analysis time. Additional benefits of this biosensing technique include the lack of contact between electrodes and measurement matrix. As a result, the charge transfer parameter is negligible, and no redox probes are required. Measurements can be performed with a sample volume of 50 μL without the need for sample dilution for rapid analysis. The biosensor fabrication methodology can be adapted to the measurement of any other analytes where the binding partner can be obtained.

The administration of staurosporine increased apoptotic activity in CHO cells. We were able to measure significant increase in caspase-9 activity and caspase-9 concentration as early as 3 h after drug exposure. Therefore, potentially our impedimetric approach may serve as a practical tool for the sensitive, precise and real-time detection of apoptotic cells, complementing the state-of-the-art strategies for apoptosis detection. The current set of experiments was conducted in a simple 2D cell culture system and may not accurately reflect the cell state of CHO cells in suspension in larger bioreactors. Further work is being carried out to fully evaluate the sensor in conditions that more closely mimic the bioreactor environment and improve the reproducibility of the sensor fabrication, particularly through the automation of the process.

Institutional review board statement

Not applicable.

Informed consent statement

Not applicable.

Funding

Financial support from the University of the West of England, Bristol, United Kingdom, University College London, London, United Kingdom and Engineering and Physical Sciences Research Council (Grant: EP/L015218/1), is gratefully acknowledged.

CRediT authorship contribution statement

Boyang Chen: Conceptualization, Investigation, Methodology, Formal analysis, Writing – original draft, Supervision. **Janice Kiely:** Writing – review & editing, Supervision. **Ibidapo William:** Conceptualization, Methodology. **Richard Luxton:** Writing – review & editing, Supervision.

Declaration of Competing Interest

The authors declare that they have no known competing financial interests or personal relationships that could have appeared to influence the work reported in this paper.

Data availability

Data will be made available on request.

Acknowledgments

We would also like to thank Dr David Patton for help with SEM operation.

Appendix A. Supplementary material

Supplementary data to this article can be found online at https://doi.org/10.1016/j.bioelechem.2023.108456.

References

[1] S.W. Harcum, K.H. Lee, CHO cells can make more protein, Cell Syst. 3 (2016) 412–413, https://doi.org/10.1016/j.cels.2016.11.007.
[2] B. Krampe, M. Al-Rubeai, Cell death in mammalian cell culture: molecular mechanisms and cell line engineering strategies, Cytotechnology 62 (2010) 175–188.
[3] M. Al-Rubeai, R.P. Singh, Apoptosis in cell culture, Curr. Opin. Biotechnol. 9 (1998) 152–156.
[4] Y.Y.C. Wei, et al., Proteomics analysis of chinese hamster ovary cells undergoing apoptosis during prolonged cultivation, Cytotechnology 63 (2011) 663–677.
[5] H.F. Liu, J. Ma, C. Winter, R. Bayer, Recovery and purification process development for monoclonal antibody production, mAbs 2 (2010) 480–499, https://doi.org/10.4161/mabs.2.5.12645.
[6] H.L. Tang, H.M. Tang, M.C. Fung, J.M. Hardwick, In vivo Caspase tracker biosensor system for detecting anastasis and non-apoptotic caspase activity, Sci. Rep. 5 (2015) 1–7.
[7] C.Y. Yun, et al., Specific inhibition of caspase-8 and -9 in CHO cells enhances cell viability in batch and fed-batch cultures, Metab. Eng. 9 (2007) 406–418.
[8] M. Brentnall, L. Rodriguez-Menocal, R.L. De Guevara, E. Cepero, L.H. Boise, Caspase-9, caspase-3 and caspase-7 have distinct roles during intrinsic apoptosis, BMC Cell Biol. 14 (2013) 32.
[9] L.E. Edgington-Mitchell, M. Bogyo, Detection of active caspases during apoptosis using fluorescent activity-based probes, in: Methods in Molecular Biology, Vol. 1419, Humana Press Inc., 2016, pp. 27–39.
[10] Y. Pan, et al., Colorimetric detection of apoptosis based on caspase-3 activity assay using unmodified gold nanoparticles, Chem. Commun. 48 (2012) 997–999.
[11] Y. Li, Chemiluminescent determination of the activity of caspase-3 using a specific peptide substrate and magnetic beads, Microchim. Acta 177 (2012) 443–447.
[12] C. Chen, M. La, Recent developments in electrochemical, electrochemiluminescent, photoelectrochemical methods for the detection of Caspase-3 activity, Int. J. Electrochem. Sci. 15 (2020) 6852–6862.
[13] H. Chen, et al., Fabrication of a protease sensor for caspase-3 activity detection based on surface plasmon resonance, Analyst 138 (2013) 5757–5761.
[14] D. Deng, et al., A signal-on electrochemical biosensor for evaluation of caspase-3 activity and cell apoptosis by the generation of molecular electrocatalysts on graphene electrode surface for water oxidation, Sens Actuat. B: Chem. 286 (2019) 415–420.
[15] J.S. Daniels, N. Pourmand, Label-free impedance biosensors: opportunities and challenges, Electroanalysis 19 (2007) 1239.
[16] N. Xia, et al., Impedimetric biosensor for assay of caspase-3 activity and evaluation of cell apoptosis using self-assembled biotin-phenylalanine network as signal enhancer, Sens Actuat. B: Chem. 320 (2020), 128436.
[17] N. Xia, et al., Protease biosensor by conversion of a homogeneous assay into a surface-tethered electrochemical analysis based on streptavidin-biotin interactions, ACS Sens. 6 (2021) 1166–1173.
[18] D. Wu, et al., Electrochemical determination of caspase-3 using signal amplification by HeLa cells modified with silver nanoparticles, Microchim. Acta 188 (2021) 1–8.
[19] C. Zhang, et al., Sandwich-type electrochemical immunosensor for sensitive detection of CEA based on the enhanced effects of Ag NPs@CS spaced Hemin/rGO, Biosens. Bioelectron. 126 (2019) 785–791.
[20] Q. Liu, J. Wang, B.J. Boyd, Peptide-based biosensors, Talanta 136 (2015) 114–127.
[21] R.A. Dorledo de Faria, L.G. Dias Heneine, T. Matencio, Y. Messaddeq, Faradaic and non-faradaic electrochemical impedance spectroscopy as transduction techniques for sensing applications, Int. J. Biosens. Bioelectron. 5 (2019).
[22] J. Shi, D. Marshall, Surface modification approaches for electrochemical biosensors, in: Biosensors - Emerging Materials and Applications, InTech, 2011, doi: 10.5772/17770.
[23] N.R. Shanmugam, S. Muthukumar, S. Prasad, A review on ZnO-based electrical biosensors for cardiac biomarker detection, Future Sci. OA 3 (2017), FSO196.
[24] R. Yakimova, et al., ZnO materials and surface tailoring for biosensing, Front. Biosci. - Elite 4 E (2012) 254–278.
[25] J.E. Lee, et al., ZnO-CuO core-hollow cube nanostructures for highly sensitive acetone gas sensors at the PPB level, ACS Appl. Mater. Interfaces 12 (2020) 35688–35697.
[26] L. Cao, J. Kiely, M. Piano, R. Luxton, Nanoparticle-based 3D membrane for impedimetric biosensor applications, Bioelectrochemistry 136 (2020), 107593.
[27] L. Cao, J. Kiely, M. Piano, R. Luxton, A copper oxide/zinc oxide composite nano-surface for use in a biosensor, Materials 12 (2019).
[28] N. Batra, M. Tomar, V. Gupta, ZnO-CuO composite matrix based reagentless biosensor for detection of total cholesterol, Biosens. Bioelectron. 67 (2015) 263–271.
[29] H. Ma, et al., An impedance-based integrated biosensor for suspended DNA characterization, Sci. Rep. 3 (2013) 1–7.
[30] A. Gasser, J. Eveness, J. Kiely, D. Attwood, R. Luxton, A non-contact impedimetric biosensing system for classification of toxins associated with cytotoxicity testing, Bioelectrochemistry 133 (2020), 107448.
[31] A.P. Haring, et al., 3D bioprinting using hollow multifunctional fiber impedimetric sensors, Biofabrication 12 (2020), 035026.
[32] A.S. Tanak, B. Jagannath, Y. Tamrakar, S. Muthukumar, S. Prasad, Non-faradaic electrochemical impedimetric profiling of procalcitonin and C-reactive protein as a dual marker biosensor for early sepsis detection, Anal. Chim. Acta X 3 (2019), 100029.
[33] Y. Yusof, Y. Yanagimoto, S. Uno, K. Nakazato, Electrical characteristics of biomodified electrodes using nonfaradaic electrochemical impedance spectroscopy (2011), Preprint at https://www.semanticscholar.org/paper/Electrical-characteristics-of-biomodified-using-Yusof-Yanagimoto/40ba9dbceb1d936e41a4070773c368c6de936fab.
[34] H. Deniz, Z. Onur, Impedimetric biosensors for label-free and enzymless detection, in: State of the Art in Biosensors - General Aspects, InTech, 2013, doi: 10.5772/52169.
[35] S.C. Perry, S.M. Gateman, J. Sifakis, L. Pollegioni, J. Mauzeroll, Enhancement of the enzymatic biosensor response through targeted electrode surface roughness, J. Electrochem. Soc. 165 (2018) G3074–G3079.
[36] M.O. Fatehah, H.A. Aziz, S. Stoll, Stability of ZnO nanoparticles in solution. Influence of pH, dissolution, aggregation and disaggregation effects, J. Colloid Sci. Biotechnol. 3 (2014) 75–84.
[37] V.S. Sousa, M.R. Teixeira, Aggregation kinetics and surface charge of CuO nanoparticles: the influence of pH, ionic strength and humic acids, Environ. Chem. 10 (2013) 313.
[38] G. Li, et al., Purification of human immunoglobulin G: a new approach to plasma fractionation, Vox Sang. 83 (2002) 332–338.
[39] E. Katz, I. Willner, Probing biomolecular interactions at conductive and semiconductive surfaces by impedance spectroscopy: routes to impedimetric immunosensors, DNA-sensors, and enzyme biosensors, Electroanalysis 15 (2003) 913–947.
[40] A. Oseev, M.P. Schmidt, S. Hirsch, A. Brose, B. Schmidt, Two-component dielectric dispersion impedance biosensor for in-line protein monitoring, Sens. Actuat. B: Chem. 239 (2017) 1213–1220.
[41] L. HTN, P. J., C. S, A probeless capacitive biosensor for direct detection of amyloid beta 1-42 in human serum based on an interdigitated chain-shaped electrode, Micromachines (Basel) 11 (2020).
[42] N. Couniot, L.A. Francis, D. Flandre, A 16 × 16 CMOS capacitive biosensor array towards detection of single bacterial cell, IEEE Trans. Biomed. Circuits Syst. 10 (2016) 364–374.
[43] C.A. Belmokhtar, J. Hillion, E. Ségal-Bendirdjian, Staurosporine induces apoptosis through both caspase-dependent and caspase-independent mechanisms, Oncogene 20 (2001) 3354–3362.
[44] G. Zhang, G. Yan, V. Gurtu, C. Spencer, S.R. Kain, Caspase inhibition prevents staurosporine-induced apoptosis in CHO-K1 cells, Apoptosis 3 (1998) 27–33.
[45] A. Saraste, K. Pulkki, Morphologic and biochemical hallmarks of apoptosis, Cardiovasc. Res. 45 (2000) 528–537.
[46] R. Mokhtar-Ahmadabadi, et al., Developing a circularly permuted variant of Renilla luciferase as a bioluminescent sensor for measuring Caspase-9 activity in the cell-free and cell-based systems, Biochem. Biophys. Res. Commun. 506 (2018) 1032–1039.